JOURNAL OF MATERIALS SCIENCE 15 (1980) 1841–1849

Crack velocity dependence of longitudinal fracture in bone

J. C. BEHIRI, W. BONFIELD
Department of Materials, Queen Mary College, London, E1 4NS, UK

An evaluation of the fracture characteristics of bovine tibia compact tension specimens associated with controlled crack propagation in the longitudinal direction has been made. The fracture mechanics parameters of critical strain energy release rate (G_c) and critical stress intensity factor (K_c) were determined for a range of crack velocities. A comparative fracture energy (W) was also evaluated from the area under the load–deflection curve. It was found that an increase in the average crack velocity from 1.75 to 23.6 $\times$ 10^{-5} m sec^{-1} produced increases in G_c (from 1736 to 2796 J m^{-2}), K_c (from 4.46 to 5.38 MN m$^{-3/2}$) and W. At crack velocities $> 23.6 \times 10^{-5}$ m sec^{-1}, W decreased appreciably. Microstructural observations indicated that, for crack velocities < 23.6 m sec^{-1}, relatively rough fracture surfaces were produced by the passage of the crack around intersecting osteons (or lamellae), together with some osteon pull-out. In contrast, at a higher crack velocity, fracture was characterized by relatively smooth surfaces, as the crack moved indiscriminately through the microstructural constituents.

1. Introduction

The anisotropy of the microstructure of compact bone in the major support bones, i.e. with osteons aligned in a preferred orientation parallel to the longitudinal axis of the bone, produces a corresponding anisotropy in the fracture characteristics [1]. At a given strain rate, it requires a smaller stress, or energy, to fracture bone sections in the longitudinal direction (i.e. mainly between the osteons) than in the transverse direction (i.e. mainly across the osteons). Compact bone is also notch sensitive and the presence of surface cracks significantly reduces the energy absorbed during fracture for both longitudinal and transverse fracture directions [2]. A variety of fracture mechanics techniques have been utilized to assess the fracture toughness of bone specimens with a "characterized" crack, which have included measurements of the critical strain energy release rate (G_c) (or the specific surface energy γ, $= G_c/2$), and the critical stress intensity factor, K_c [3–6]. The specimen geometries used in these earlier experiments all produced rapid crack propagation, with an unknown and variable crack velocity. More recently, in contrast, with the use of the compact tension test method [7], it has been possible to propagate a crack in bone at a relatively slow and measurable rate and G_c and K_c values for transversely oriented bovine femur bone specimens were determined by this method for a range of crack velocities [8]. The results of these investigations are shown for comparison in Table I.

In the current investigation, the compact tension specimen approach has been extended to evaluate the fracture of transversely oriented (i.e. with fracture in the longitudinal direction) bovine tibia compact bone specimens, in terms of G_c and K_c, for a range of cross-head speeds from 1.7 to 170×10^{-7} m sec^{-1}. These fracture mechanics results were correlated with the bone fracture profiles and surfaces observed by optical and scanning electron microscopy.

2. Experimental procedure

Typical sections of compact bone from the adult bovine tibias investigated in this study are shown in Fig. 1. Transversely oriented compact tension specimens (i.e. with the starter crack introduced parallel to the long axis of the bone and the fracture plane corresponding to the surface shown in

0022–2461/80/071841–09$02.90/0

TABLE I Some previous investigations of the fracture mechanics parameters for bone

Investigation	Method	Orientation*	Bone type	G_c ($J\,m^{-2}$)	K_c ($MN\,m^{-3/2}$)
Melvin and Evans [3]	Single-edge notched	Transverse	Bovine femur	1388–2557	3.21
		Longitudinal	Bovine femur	3135–5534	5.58
Margel-Robertson [4]	Three-point bending	Longitudinal	Bovine femur	–	6.56
Bonfield and Datta [5]	Centre notched (shock tube)	Transverse	Bovine tibia	4	0.23
Bonfield and Datta [6]	Single-edge notched	Longitudinal	Bovine tibia	780–1120	2.2–4.6
Wright and Hayes [7]	Compact tension	Transverse	Bovine femur	820	3.5
Bonfield *et al.* [8]	Compact tension	Transverse	Bovine femur	920–2780	2.4–5.2

* A *transverse* specimen orientation produces fracture in the *longitudinal* direction.
A *longitudinal* specimen orientation produces fracture in the *transverse* direction.

Fig. 1b), were wet machined from the mid-diaphysis and were stored in Ringers solution at -20° C until tested. A typical compact tension specimen is shown in Fig. 2.

The test specimens were mounted in an Instron testing machine and subsequently loaded at room temperature at cross-head speeds ranging from 1.7 to 170×10^{-7} m sec^{-1} until crack propagation occurred, care being taken to keep the bone specimens saturated with Ringers solution during the tests.

The decrease in load (P) associated with crack propagation was measured on the Instron chart recorder, while the extension of the crack with time (hence crack velocity) was measured microscopically. The fractured specimens were examined optically under reflected light to establish the fracture profile and its relationship to the microscopic structure, while the fracture surface was examined with a JEOL-JXA 50A scanning electron probe microanalyser.

A compliance calibration was performed after forming a crack with a razor blade at the specimen mid-point. The length of the crack was accurately measured with a travelling microscope. The specimen was then loaded (with no crack propagation) and unloaded and the average slope of the graph calculated. The crack was incrementally lengthened and the process repeated for a series of crack lengths corresponding to a/w ratios from 0.32 to 0.70 where a is the crack length and w is the specimen width. This technique was repeated for other specimens at different cross-head speeds. The compliance calibration curve was then established by a plot of C versus a, where the compliance C is related to the load (P) and deflection (d) by

$$C = d/P. \quad (1)$$

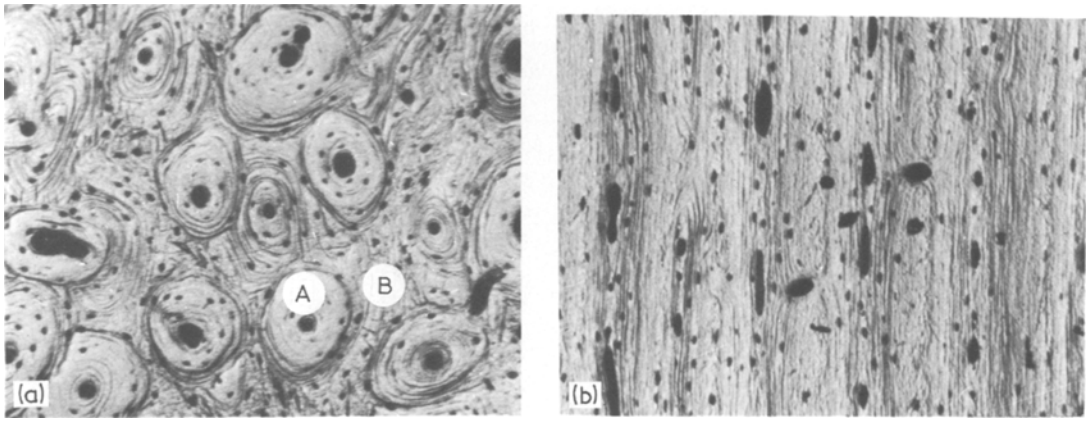

Figure 1 Reflected-light micrographs of polished sections of adult bovine tibia compact bone, (a) perpendicular to the long axis, showing mainly cylindrical cross-sections of longitudinally aligned osteons (A), with concentric lamellae of hydroxyapatite and collagen and a central Haversian canal, and a small number of elliptical cross-sections of osteons at different orientations to the long axis, together with non-orientated interstitial bone (B), and (b) parallel to the long axis, showing mainly sections through the longitudinally aligned osteons and a few cylindrical and elliptical cross-sections of intersecting osteons (× 84).

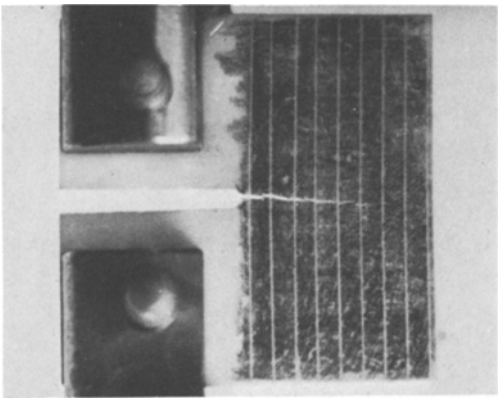

Figure 2 Compact tension test specimen (× 1.5) mounted in the grips of an Instron testing machine, showing crack propagation (with the surface darkened with carbon to improve contrast) from a machined crack. The critical dimensions are the width ($w = 26$ mm), the machined crack length (a), (both measured from the vertical axis through the locating pins) and the thickness ($B = 2$ mm).

The expression for the critical strain energy release rate, G_c, is given by:

$$G_c = \frac{P^2}{2B}\left(\frac{\partial C}{\partial a}\right) \tag{2}$$

where B is specimen thickness, P is the load, C the compliance and a the crack length, while the expression for the critical stress intensity factor (K_c) for the compact tension specimen [9] is given by:

$$K_c = \frac{P}{Bw^{1/2}} Y_2 \tag{3}$$

where

$$Y_2 = 29.6\left(\frac{a}{w}\right)^{1/2} - 185.5\left(\frac{a}{w}\right)^{3/2} + 655.7\left(\frac{a}{w}\right)^{5/2} - 1017\left(\frac{a}{w}\right)^{7/2} + 638.9\left(\frac{a}{w}\right)^{9/2}. \tag{4}$$

The crack profile was assessed by metallographic polishing and optical microscope examination of the side surfaces of the fractured specimens. The partially fractured specimens were then pulled apart revealing the fracture surfaces, which were sputter coated with gold/palladium prior to examination in the scanning electron probe microanalyser.

3. Results

3.1. Compact tension tests

A typical load–deflection record is shown in Fig. 3, which reveals an initial region of increasing slope, followed by a linear region until the crack started to propagate and the load progressively

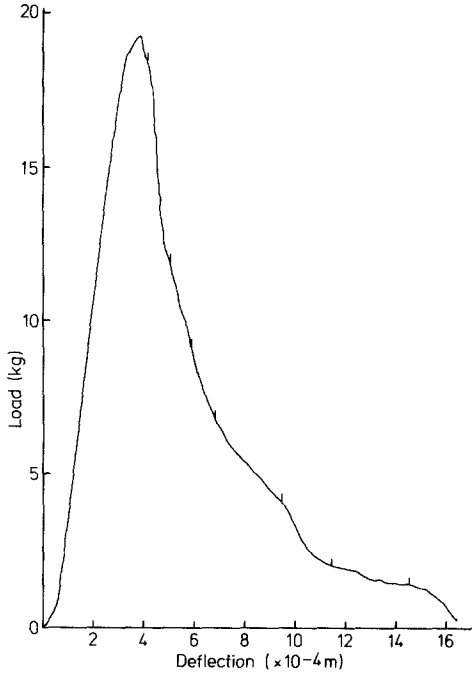

Figure 3 Instron chart recording of load (P) versus deflection (d).

decreased as the crack length increased. The "blip" markers on the curve correspond to the times at which the crack front reached scribed distance markers on the specimen surface (spaced at 2 mm). In these tests, the average crack velocity was taken between the first marker and the final crack position.

Load–deflection curves were measured in the linear region prior to crack propagation for a variety of starting crack lengths (Fig. 4). The reciprocal slopes from Fig. 4 were used to construct a compliance calibration curve (Fig. 5), from which the slope $\partial C/\partial a$ at a given crack length a, was determined as the tangent of the compliance curve at that point.

During the region of crack propagation, shown

TABLE II Derivation of G_c and K_c from experimental measurements of P and a

a (mm)	P (kg)	$\partial C/\partial a$ (N^{-1})	G_c ($J\,m^{-2}$)	K_c ($MN\,m^{-3/2}$)
8.5	16.4	0.7	559	3.3
10.5	15.2	1.8	1111	3.7
12.5	12.6	2.8	1188	3.7
14.5	9.5	4.8	1145	3.5
16.5	8.6	7.5	1482	4.2
18.5	6.6	22	2514	4.7

Cross-head speed 1.7×10^{-7} m sec^{-1}.
$B = 1.8$ mm $w = 26.5$ mm.

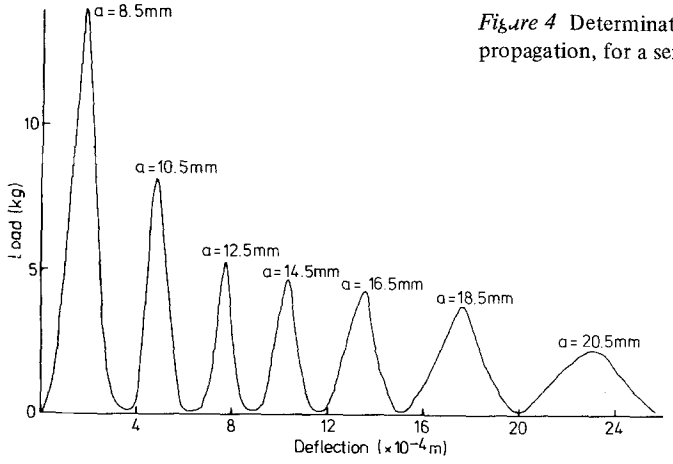

Figure 4 Determination of load–deflection curves, prior to crack propagation, for a series of existing crack lengths (a).

in Fig. 3, values of load (P) were determined as the crack length (a) increased. Test values of P and a are given in Table II for one specimen tested at a cross-head speed of 1.7×10^{-7} m sec^{-1}, from which, with $\partial C/\partial a$ determined from the compliance calibration curve (Fig. 4), values of G_c and K_c were calculated (and are shown in Table II). This procedure was repeated for three different specimens and average values of G_c and K_c determined. For each specimen, the initial values of G_c and K_c (at $a = 8.5$ mm) were not included in the averages, as it was considered that these results were associated with the starter crack rather than the propagating crack. With this exception, the averages for all other values were not significantly different to those confined within the suggested test limits of $0.45 < a/w < 0.55$ [9]. Similar tests were then performed at various cross-head speeds from 1.7 to 84×10^{-7} m sec^{-1}. It was found, as listed in Table III, that an increase in cross-head speed in this range increased the average crack velocity and the average values of G_c and K_c. If the cross-head speed was increased above this range, e.g. to the next available cross-head speed (170×10^{-7} m sec^{-1}), then fracture occurred at a considerably increased crack velocity, such that measurement of the crack velocity by the microscopic technique was not possible (referred to subsequently as catastrophic fracture). The instantaneous decrease in P also precluded a determination of G_c and K_c. However, the decrease in the energy associated with fracture at this cross-head speed was demonstrated from measurements of the areas under the various load–deflection curves, which, divided by twice the fracture surface area in each case, gave a comparative evaluation of fracture energy (W). The variation in fracture energy (W) defined in this manner with cross-head speed is shown in Table III.

3.2. Fractography

A typical fracture profile of the intersection of the crack with one side face of the specimen during slow crack propagation is shown in Fig. 6, which illustrates the relation of the crack path to various intersecting osteons, mainly with central axes

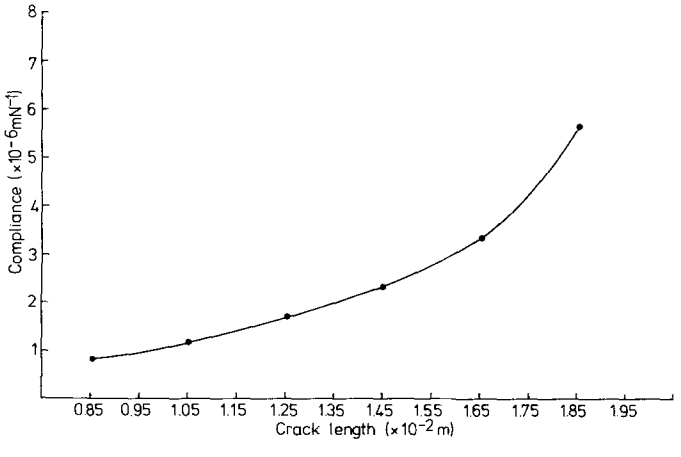

Figure 5 Compliance calibration curve.

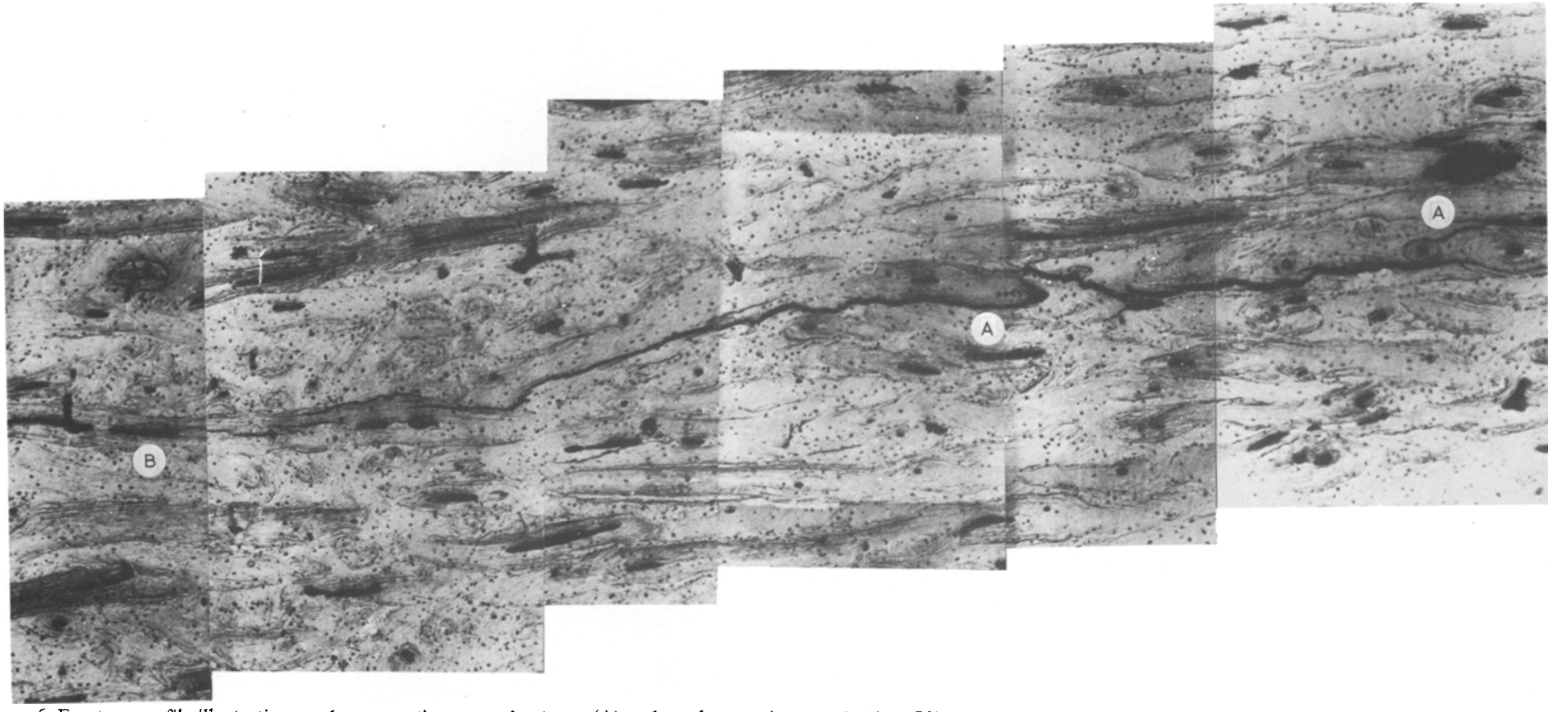

Figure 6 Fracture profile illustrating crack propagation around osteons (A) and crack arrest in a canal (B) (× 72).

TABLE III Average values of G_c, K_c and W obtained by various crack velocities

Cross head speed ($\times 10^{-7}$ m sec^{-1})	Average crack velocity ($\times 10^{-5}$ m sec^{-1})	Average G_c (J m^{-2})	Average K_c (MN m$^{-3/2}$)	Average W J m^{-2}
1.7	1.75	1736	4.46	764
3.3	1.95	1753	4.61	1314
8.4	3.60	1806	5.02	1345
17.0	7.60	2110	5.04	1562
33.0	12.60	2254	5.23	1900
84.0	23.55	2796	5.38	2125
170.0*	–	–	–	125

* Catastrophic crack propagation.

aligned parallel (or at small angles) to the fracture plane. The passage of the crack around the periphery of intersecting osteons, i.e. along the osteon–interstitial bone interface, is evident in Fig. 6, together with crack arrest in an intersecting Haversian canal. In addition, some interlamellar fracture within the outer-most lamellae of the intersecting osteons can be distinguished, as shown at higher magnification in Fig. 7.

The fracture surfaces obtained under the two extreme conditions of crack propagation are shown in Fig. 8, with a low propagation associated with a relatively rough surface (Fig. 8a), and rapid propagation, characterized by a relatively smooth and flat surface (Fig. 8b). Observation of the fracture surface revealed crack propagation across the occasional intersecting osteon, with a central axis normal (or at a large angle) to the fracture plane, such as shown in Fig. 9. The individual lamellae can be resolved and it is apparent that the crack propagated sequentially, first, circumferentially along the osteon–interstitial bone interface normal (or at a large angle) to the general fracture plane, then across the adjacent lamella parallel (or at a small angle) to the general fracture plane, along the next interlamellar interface, across the next lamella and so on. As the distance from the general fracture plane increased, so the interlamellar fracture distance travelled decreased, with, in the limit, fracture across several neighbouring lamellae around the Haversian canal, with a resultant conical fracture and a form of osteon pull-out.

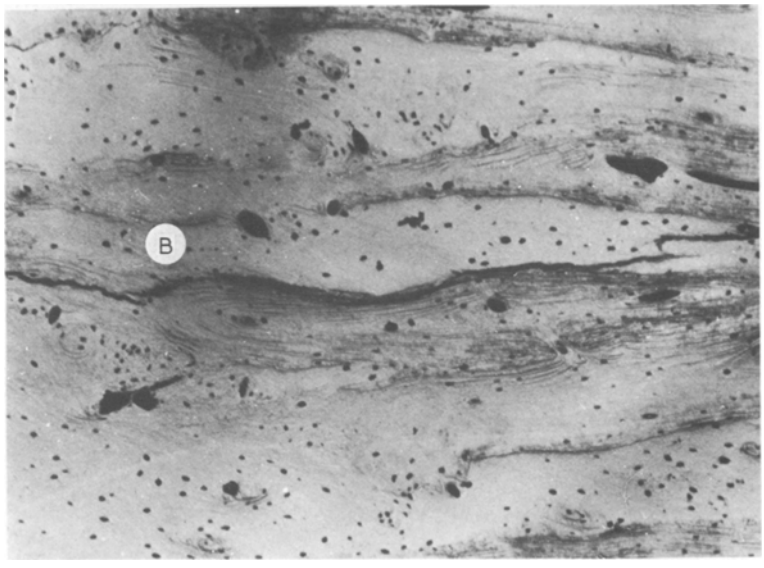

Figure 7 Crack propagation around osteons with some interlamellar fracture (B) (× 160).

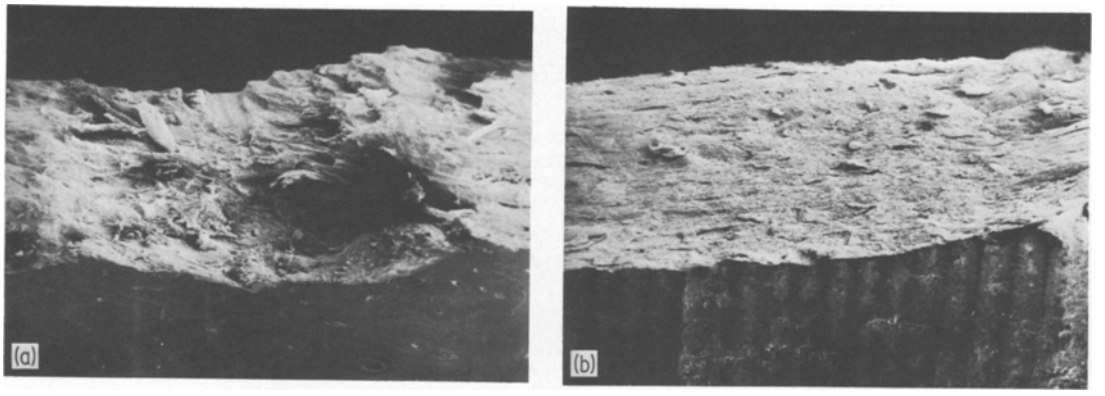

Figure 8 Fracture surface after (a) slow crack propagation (× 34) and (b) after rapid crack propagation (× 34).

4. Discussion

The results of the present study indicate that the fracture mechanics parameters of critical strain energy release rate (G_c) and critical stress intensity factor (K_c) for bovine tibia specimens increase with increases in the cross-head speed and crack velocity in the controlled crack propagation region. It can be seen from Table III that an increase in the cross-head speed from 1.7 to 84×10^{-7} m sec^{-1} resulted in an increase in the average crack velocity from 1.75 to 23.5×10^{-5} m sec^{-1} and that increases in crack velocity within this range produced small, but systematic, increases in the average G_c, from 1736 to 2796 J m^{-2} and in the average K_c, from 4.46 to 5.38 MN m$^{-3/2}$. Similar trends for G_c and K_c were observed in a study of bovine femur compact tension specimens [8], although comparable increases in crack velocity within the limits of 2.1 to 27×10^{-5} m sec^{-1}, produced somewhat larger increases in G_c from 920 to 2780 J m^{-2} and in K_c from 2.4 to 5.2 MN m$^{-3/2}$. Fig. 10 illustrates the comparison between the two investigations. The catastrophic crack propagation obtained at a higher cross-head speed of 170×10^{-5} m sec^{-1}, precluded an assessment of G_c and K_c. However, a previous study of transversely oriented bovine tibia sections, with fracture produced by shock loading [5],

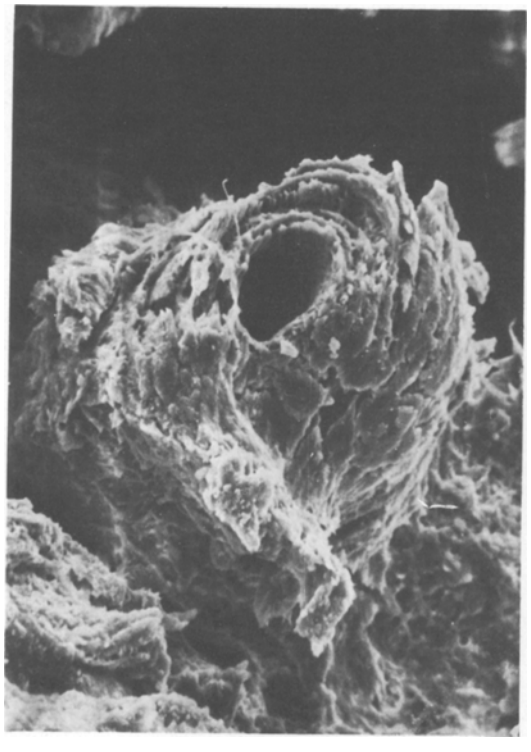

Figure 9 Portion of fracture surface with osteon pull-out (× 780).

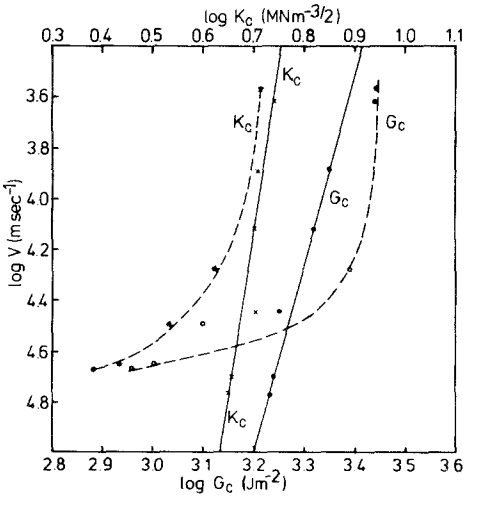

Figure 10 The dependence of critical strain energy release rate (G_c) and critical stress intensity factor (K_c) on crack velocity. The current results for bovine tibia specimens (———) are compared with the results of Bonfield *et al.* [7] for bovine femur specimens (– – – –).

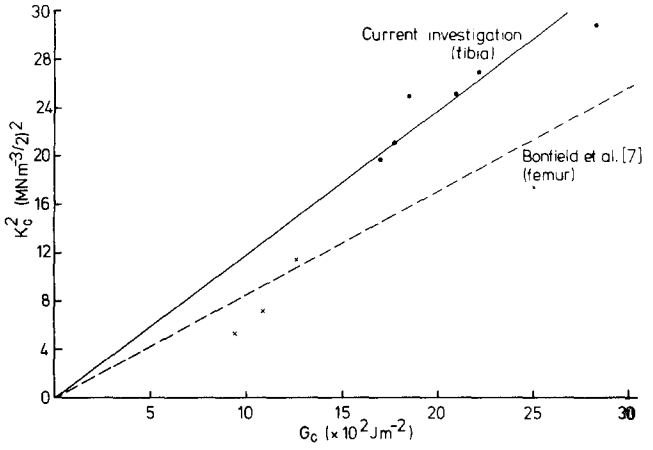

Figure 11 The relationship between K_c^2 and G_c for bovine tibia specimens (——) and bovine femure specimens (– – – –) [7].

indicated that significantly smaller values of G_c and K_c are associated with catastrophic crack propagation (see Table I).

For the case of isotropic materials in plain strain, the two fracture mechanics parameters K_c and G_c are related by the expression:

$$K_c^2 = \frac{E}{1-\nu^2} G_c \qquad (5)$$

where E and ν are, respectively, the transverse Young's modulus and Poissons ratio. Compact bone is not isotropic, but for transversely oriented bone specimens, with mainly interosteonal fracture, then Equation 5 provides a reasonable approximation [8]. Fig. 11 shows the variation between the average values of G_c and K_c^2 derived for the six cross-head speeds and gives a slope, $E/(1-\nu^2)$, of $12.0\,\mathrm{GN\,m^{-2}}$ and hence taking $\nu = 0.2$, $E = 11.5\,\mathrm{GN\,m^{-2}}$. This value of E is similar to other derived values of Young's modulus for bone of $9.4\,\mathrm{GN\,m^{-2}}$ [7] and $8.8\,\mathrm{GN\,m^{-2}}$ [8], as well as to experimentally determined values of E for the transverse orientation, e.g. $7.2\,\mathrm{GN\,m^{-2}}$ [1] and 8.7 to $10.3\,\mathrm{GN\,m^{-2}}$ [10].

The results obtained between cross-head speed and fracture energy (W) assessed from the area under the load–deflection curve demonstrate that, in a similar manner to G_c and K_c, W also increases significantly with cross-head speed, from $764\,\mathrm{J\,m^{-2}}$ at a cross-head speed of $1.7 \times 10^{-7}\,\mathrm{m\,sec^{-1}}$ (and average crack velocity of $1.75 \times 10^{-5}\,\mathrm{m\,sec^{-1}}$) to $2125\,\mathrm{J\,m^{-2}}$ at a cross-head speed of $84 \times 10^{-7}\,\mathrm{m\,sec^{-1}}$ (an average crack velocity of $23.5 \times 10^{-5}\,\mathrm{m\,sec^{-1}}$). Above these limits of cross-head speed and crack velocity, a transition from slow to catastrophic crack propagation occurred, resulting in a sudden decrease in W to $125\,\mathrm{J\,m^{-2}}$. The existence of a critical cross-head speed, above which fracture occurs catastrophically, with a reduced value of energy (W) (as defined from a load–deflection curve), has been demonstrated previously for the transverse fracture direction and the values determined (e.g. $2.1 \times 10^{-6}\,\mathrm{m\,sec^{-1}}$ [4], $4.2 \times 10^{-6}\,\mathrm{m\,sec^{-1}}$ [11]) are comparable to that in the present study. Of course, a given cross-head speed may not give the same crack velocity with different test conditions and it is the crack velocity which, it is suggested, is of fundamental significance. However, the crack velocity associated with this critical cross-head speed has not been generally established, but the current results indicate a higher critical velocity in the longitudinal direction than would perhaps be expected from an earlier assessment of the critical velocity in the transverse direction ($1.6 \times 10^{-6}\,\mathrm{m\,sec^{-1}}$ [12]). The absolute values of W reported in Table III are significantly lower than these previous studies, which is attributed to the different orientations of the specimens (i.e. the transverse specimen orientation in the present study produces fracture along the weaker longitudinal direction).

The transition from controlled crack propagation to catastrophic fracture was correlated with a change in the fracture characteristics from relatively rough surfaces reflecting the microstructural features to relatively smooth fracture surfaces. The fracture modes observed in the controlled crack propagation region, namely interosteonal, interlamellar and intraosteonal fracture, are similar to those originally defined for fracture in the transverse direction [12], although with smaller excursions from the fracture plane and less osteon pull-out. It is interesting to note

that osteon pull-out is also different in detail, with a conical rather than cylindrical form [11]. These fractography results demonstrate that, although the preferred orientation of the central axes of the osteons is along the longitudinal axis of the bone (and the crack direction), there are sufficient osteons aligned in other directions to modify the crack path. The crack arrest observed in Haversian canals is attributed to crack "blunting" by effectively increasing the radius of curvature of the crack tip and hence requiring an increase in the stress intensity factor for continued movement [6]. At this stage, the variation in G_c, K_c and W for different crack velocities *within* the controlled crack propagation range could not be correlated with differences in the various microstructural fracture modes.

5. Conclusions

(1) Transversely oriented bovine tibia compact tension specimens exhibited slow crack propagation when deformed at cross-head speeds within the range 1.7 to 84×10^{-7} m sec^{-1}.

(2) An increase in cross-head speed within the limits of 1.7 to 84×10^{-7} m sec^{-1} produced increases in the crack velocity from 1.75 to 23.6×10^{-5} m sec^{-1}.

(3) Within the crack velocities recorded, the critical strain energy release rate (G_c) varied from 1736 to 2796 J m^{-2} and the critical stress intensity factor (K_c) from 4.46 to 5.38 MN m$^{-3/2}$.

(4) An increase in cross-head speed within the limits of 1.7 to 84×10^{-7} m sec^{-1} resulted in an increase in the fracture energy (W) from 764 to 2125 J m^{-2}. At a cross-head speed of 170×10^{-7} m sec^{-1}, W decreased to 125 J m^{-2}.

(5) With controlled crack propagation, a relatively rough fracture surface was produced by the passage of the crack around intersecting osteons (or lamellae), together with some osteon pull-out.

(6) With catastrophic crack propagation, the crack moved indiscriminately through the microstructural constituents of bone and the fracture surfaces were relatively smooth.

Acknowledgement

The authors gratefully acknowledge the provision of a research grant and research studentship (JCB) by the Science Research Council.

References

1. F. G. EVANS, "Mechanical Properties of Bone" (Albert C. Thomas, Springfield, Illinois, 1972).
2. W. BONFIELD and C. H. LI, *J. Appl. Phys.* **37** (1966) 869.
3. J. W. MELVIN and F. G. EVANS, ASME, Biomaterials Symposium, Detroit, MI (1973).
4. D. MARGEL ROBERTSON, Ph.D. Thesis, University of Stanford, California (1973).
5. W. BONFIELD and P. K. DATTA, *J. Mater. Sci.* **9** (1974) 1609.
6. *Idem, J. Biomechanics* **9** (1976) 131.
7. T. M. WRIGHT and W. HAYES, *ibid* **10** (1977) 419.
8. W. BONFIELD, M. D. GRYNPAS and R. J. YOUNG, *ibid* **11** (1978) 473.
9. W. BROWN and J. SRAWLEY, ASTM, SP 410 (1966).
10. W. BONFIELD and M. D. GRYNPAS, *Nature* **270** (1977) 453.
11. D. D. MOYLE, J. W. WELBORN and F. W. COOKE, *J. Biomechanics* **11** (1978) 435.
12. K. PIEKARSKI, *J. Appl. Phys.* **41** (1970) 215.

Received 27 November and accepted 14 December 1979.